JACS
JOURNAL OF THE AMERICAN CHEMICAL SOCIETY
pubs.acs.org/JACS

Open Access
This article is licensed under CC-BY 4.0

Communication

Band Gap Narrowing by Suppressed Lone-Pair Activity of Bi^{3+}

Kanta Ogawa,* Ryu Abe, and Aron Walsh

Cite This: J. Am. Chem. Soc. 2024, 146, 5806−5810

Read Online

ACCESS | Metrics & More | Article Recommendations | Supporting Information

ABSTRACT: Post-transition metal cations with a lone pair (ns^2np^0) electronic configuration such as Pb^{2+} and Bi^{3+} are important components of materials for solar-to-energy conversion. As in molecules like NH_3, the lone pair is often stereochemically active in crystals, associated with distorted coordination environments of these cations. In the present study, we demonstrate that suppressed lone pair stereochemical activity can be used as a tool to enhance visible light absorption. Based on an orbital interaction model, we predict that a centrosymmetric environment of the cations limits the orbital interactions with anions, deactivates the lone pair, and narrows the band gap. A high-symmetry Bi^{3+} site is realized by isovalent substitutions with Y^{3+} by considering its similar ionic radius and absence of a lone pair. The quaternary photocatalyst Bi_2YO_4X is singled out as a candidate for Bi substitution from a survey of the coordination environments in Y−O compounds. The introduction of Bi^{3+} to the undistorted Y^{3+} site in Bi_2YO_4X results in a narrowed band gap, as predicted theoretically and confirmed experimentally. The orbital interaction controlled by site symmetry engineering offers a pathway for the further development of post-transition metal compounds for optoelectronic applications.

Downloaded via IMPERIAL COLLEGE LONDON on August 16, 2024 at 21:15:49 (UTC).
See https://pubs.acs.org/sharingguidelines for options on how to legitimately share published articles.

Semiconductors containing post-transition metal cations with a lone pair (ns^2np^0) electronic configuration (Sn^{2+}, Sb^{3+}, Pb^{2+}, Bi^{3+}) are a special class of photoabsorbers in solar-to-energy conversion systems.[1−4] The filled s orbitals interact with anion orbitals to form the upper valence band, providing unique optoelectronic properties such as defect tolerance,[5] reduced hole effective mass,[6,7] and shallow ionization potentials. These effects have led to promising photo(electro)-catalysts such as $BiVO_4$,[8,9] Bi_4NbO_8Cl,[10,11] and $Pb_2Ti_2O_{5.4}F_{1.2}$.[12]

The orbital interactions in these materials can be described within the revised lone-pair model,[1] which explains the asymmetric coordination environment of these cations in many crystal structures.[13−18] The metal s−anion p interactions create filled bonding and antibonding combinations as illustrated in Figure 1. The antibonding combination further interacts with the empty metal p orbitals.

The extent of the metal p orbital mixing is influenced by the coordination environment of the cation. At an asymmetric site, the mixing is favorable as shown in Figure 1a, providing the stereochemically active lone pair. The distorted cation coordination environments stabilize the valence band maximum (VBM) and enlarge band gap as seen in δ-Bi_2O_3[19,20] and $SnWO_4$.[21] Conversely, we posit that when a lone pair cation is placed at a high symmetry site, the band gap will be narrowed due to suppressed metal p coupling (Figure 1b). One approach to achieve a higher symmetry environment is through external force. Balic-Zunic et al. studied the effect of pressure on the crystal structure of Bi_2S_3, showing that high pressure provides a more symmetric coordination environment of Bi^{3+}.[22] A subsequent theoretical study by Olsen et al. revealed that the symmetry increase is accompanied by a reduced band gap of Bi_2S_3.[23] However, high-pressure is impractical for solar-to-chemical conversion systems. Here, we demonstrate that a high symmetry Bi^{3+} can be realized under ambient conditions, which results in a significant reduction of the band gap.

We focus on yttrium because Y^{3+} has a similar ionic radius (1.02 Å) to Bi^{3+} (1.17 Å)[24] but without the valence s^2 electrons causing the structural distortion. From the Materials Project database,[25] we searched for metal oxide crystals with Y^{3+} in a highly symmetric site and then investigated the effect of the Bi^{3+} introduction to the Y^{3+} site. We analyzed the coordination environments of Y^{3+} based on the Voronoi approach and the Continuous Symmetry Measure (CSM), where the environment is expressed as the most similar model polyhedron with the CSM value.[26] The CSM ranges from 0 (perfect polyhedron) to 100 (highly deformed). Undistorted Y^{3+} with small CSM values were found in the 6-fold octahedral (O:6) and 8-fold cubic (C:8) environments (Figure S1).

For O:6, the double perovskites Ba_2YMO_6 (M = Nb, Ta, Sb) provide regular environments (CSM = 0). The effect of Bi^{3+} substitution onto the Y^{3+} sites was investigated based on density functional theory (DFT) calculation within generalized gradient approximation. The band gaps are substantially reduced in each case (Figure S2) by 0.6−1.9 eV. The negligible Bi 6p but strong Bi 6s contributions to the VBM are consistent with our model (Figure 1b). The Bi^{3+}-based materials in the database were also analyzed (Figure S3), where the Bi^{3+} environment in Ba_2BiMO_6 (M = Sb, Ta) is slightly more distorted (CSM = 0.02, 0.03) than the Y^{3+} in the corresponding Y compound. The most distorted Bi^{3+} is accompanied by the strong Bi 6p contribution to the upper

Received: January 4, 2024
Revised: February 17, 2024
Accepted: February 20, 2024
Published: February 23, 2024

© 2024 The Authors. Published by American Chemical Society

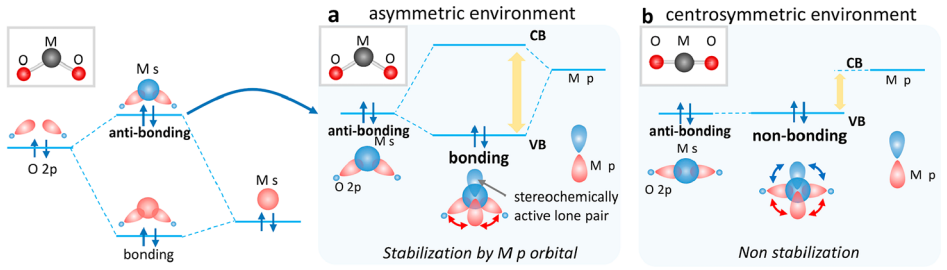

Figure 1. Illustration of the band-edge orbital interactions in lone pair containing metal oxides. The metal (M) s−anion (O) p interactions create filled bonding and antibonding combinations. (a) When the coordination environment of the cation is asymmetric, the antibonding combination is stabilized by M p coupling to form the upper valence band (VB). This results in a stereochemically active lone pair due to the M p orbital contribution to the upper VB. (b) When the coordination environment of the cation is centrosymmetric, this orbital interaction is suppressed due to destructive interference, which results in a narrower band gap. In this case, the antibonding combination between M s−O 2p mainly forms the upper VB without M p orbital contribution.

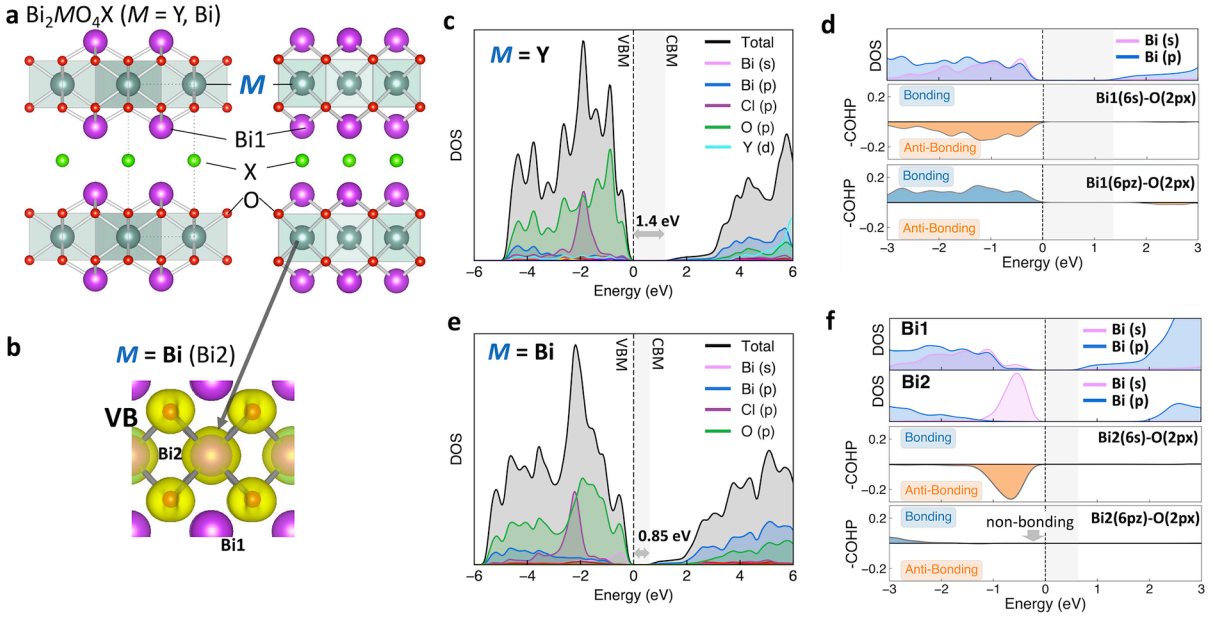

Figure 2. (a) Crystal structure of Bi_2YO_4X. (b) Charge density distribution of the upper part of the valence band (VB) for Bi_2MO_4Cl with M = Bi. The Bi at the *M* site is described as Bi2, while the Bi site in original Bi_2YO_4X is described as Bi1. Projected electronic density of states (DOS) of Bi_2MO_4Cl with M = (c, d) Y and (e, f) M = Bi with crystal orbital Hamilton populations (COHP) for Bi1 (Bi2) and O 2p. The highest occupied state (Fermi level) is set to 0 eV.

valence band (Figure S4) consistent with the orbital interaction model in Figure 1a. Note that a similar tendency can be observed for bivalent Pb^{2+} (Figure S5).

For C:8, the layered oxyhalides Bi_2YO_4X (X = Cl, Br, I; Figure 2a) show regular environments (CSM = 0).[27] The Bi introduction exerts a similar influence on their electronic structure with a band gap reduction of 0.3−0.6 eV. Note that no crystal structure was found with the CSM close to 0 in the C:8 environment of Bi^{3+}, showing that Bi^{3+} at an undistorted C:8 environment is rare (Figure S6).

We selected Bi_2YO_4X (X = Cl, I) which features a cubic Y^{3+} site as a target for Bi^{3+} introduction. The oxychloride has been reported as a water-splitting photocatalyst.[28] In Bi_2YO_4Cl, Bi1 contributes to the VBM (Figure 2c, d), in the manner expected for a stereochemically active lone pair (Figure 1a). The interactions between Bi1 and O 2p were confirmed by Crystal Orbital Hamiltonian Population (COHP) analysis (Figure 2d).[29]

The introduction of excess Bi on the Y site (i.e., forming Bi_2BiO_4Cl) significantly reduced the calculated band gap from 1.4 to 0.9 eV. The new VBM is derived from the 6s orbital of cubic Bi2. The s-orbital character around Bi2 is seen in the VBM electron density (Figure 2e, f). The COHP analysis shows the antibonding character between Bi2 6s and O 2p and nonbonding between Bi2 6p and O 2p (Figure 2f). The high-symmetry Bi^{3+} narrows the band gap by restricting the Bi6p participation to the valence band (Figure 1b). A similar tendency was observed for Bi_2YO_4I (Figure S7). It is noted that the Bi introduction to Y site negligibly affects the CBM nature because the conduction band is derived from the highly dispersive interlayer Bi1−Bi1 interaction but not from the Bi2 (Figure S8).[30]

The Bi introduction to the Y site affects other physical properties. The hole effective mass is enlarged especially in the out-of-plane direction (*c* axis) owing to the nonbonding character of the Bi2 6s orbital, while the electron effective mass is hardly affected as stated above (Table S1). The nonbonding character of Bi2 6s orbital also provides a relatively flat phonon band related to the isolated motion of Bi2; however, no imaginary modes are found (Figure S9). The Born effective

https://doi.org/10.1021/jacs.4c00150
J. Am. Chem. Soc. 2024, 146, 5806−5810

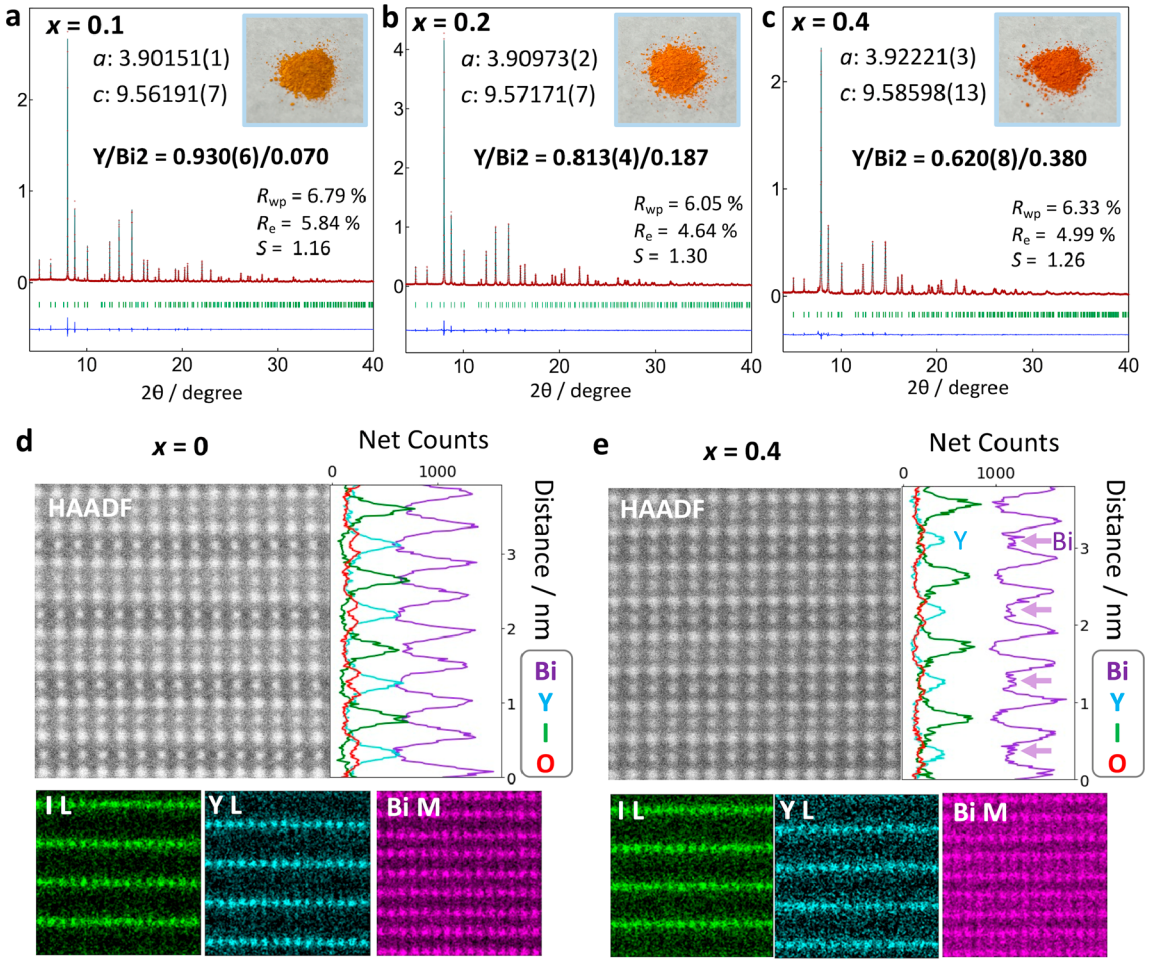

Figure 3. SXRD patterns and the Rietveld refinement profiles and product color of $Bi_2Bi_xY_{1-x}O_4I$ (x = (a) 0.1, (b) 0.2, (c) 0.4). The structure model is based on Bi_2YO_4I ($P4/mmm$).[27] HAADF images of $Bi_2Bi_xY_{1-x}O_4I$ (x = (d) 0, (e) 0.4) along the $[110]_t$ direction with STEM-EDX line scan analysis along the [001] direction and atomic resolution elemental maps for Y (light-blue), I (light-green), Bi (purple). Bi peaks can be observed around Y site in the doped sample (e).

mass of Bi2 is also more symmetric; the larger average value of Bi2 (4.8) than Y (4.2) is typical of high-polarizability lone pair cations. This will enhance the dielectric screening, which can be an advantage for charge carrier dynamics (Table S2).[31]

We experimentally introduced Bi to the Y site in Bi_2YO_4X. The Bi excess compounds, $Bi_2Bi_xY_{1-x}O_4X$, were synthesized by solid-state reaction. Doping above x = 0.5 for X = Cl and x = 0.4 for X = I provided impurity phases such as Bi_3O_4Cl and $Bi_4O_5I_2$ whose Bi site is asymmetric (Figure S10). Calculations within the quasi-harmonic approximation suggest that a dynamic instability emerges for expanded volumes at high temperatures (Figure S11). This suggests that low-temperature processing may increase the solubility of excess Bi.

Rietveld analysis of synchrotron X-ray diffraction (SXRD) patterns of the synthesized $Bi_2Bi_xY_{1-x}O_4X$ (x = 0, 0.2, 0.4, 0.5 for X = Cl, x = 0, 0.1, 0.2, 0.4 for X = I) shows the Y/Bi ratios at Y site (Bi2) consistent with x values, confirming the successful doping of Bi to the Y site (Figures 3a–c, S12, S13). The Bi-incorporation at the Y site was also supported by HAADF-EDX analysis with an increased Bi count at the Y site (Figure 3d,e) and SEM-EDX mapping (Figures S14, S15). Note that the cell volume was expanded with increasing x value because of the larger ionic radius of Bi^{3+} (Figure S16).

The Bi introduced into the Y site significantly narrows the band gap (Figure 4), accompanied by a newly formed density

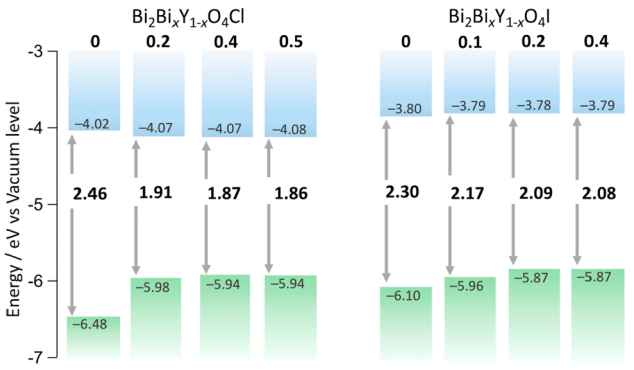

Figure 4. Band edge positions of $Bi_2Bi_xY_{1-x}O_4X$ (x = 0, 0.2, 0.4, 0.5 for X = Cl, x = 0, 0.1, 0.2, 0.4 for X = I). The lowest ionization energies obtained via photoelectron yield spectroscopy (PYS) are assumed to the valence band maximum.

of states increasing with the increased Bi ratio (Figure S17), and a change in the color of the powder (Figure 3a–c). Though a similar band gap narrowing was reported for the oxychloride system, the underlying mechanism remains elusive.[32] The band edge positions were estimated based on the lowest ionization energy obtained by photoelectron yield spectroscopy (PYS). The VBM increases with Bi doping to the

https://doi.org/10.1021/jacs.4c00150
J. Am. Chem. Soc. 2024, 146, 5806–5810

Y site (Figure 4). In Bi_2YO_4X ($x = 0$), the excess Bi causes a negative VBM shift, which is more significant in the oxychloride than the oxyiodide. For $x = 0$, the oxyiodide shows a narrower band gap than the chloride owing to the I 5p contribution to the VBM, while O 2p mainly contributes to the VBM of the chloride. In other words, in the oxyiodide, I 5p on the VBM of $x = 0$ mitigates the observed VBM shift by Bi introduction to Y, while, in the oxychloride, the effect of the change in Bi coordination environment from asymmetric (Bi1) to symmetric (Bi2) on the VBM shift can be seen. On the other hand, the CBM remains weakly affected because the conduction bands are derived from the interlayer Bi1−Bi1 interaction, whose highly dispersive nature overwhelms the contribution of the Bi2 6p to the CBM as shown in the density of states in Figure 2. The lower conduction bands of the iodides than the chlorides are derived from the larger Bi1−Bi1 distance, which results in the narrowed conduction bandwidth.[30,33]

We have demonstrated the connection between site symmetry, orbital interactions, and band gap in lone-pair-containing compounds. The predicted effects of high-symmetry Bi^{3+} sites were validated from synthetic experiments on Bi_2YO_4X with additional Bi substituted on the Y sites. This cation substitution approach can be extended to other combinations such as Sc/Sb, Ca/Sn, and Sr/Pb. Lone pair engineering offers a strategy for controlling the optoelectronic structure of the post-transition metal compounds beyond the limits of known materials.

■ ASSOCIATED CONTENT

Supporting Information

The Supporting Information is available free of charge at https://pubs.acs.org/doi/10.1021/jacs.4c00150.

Experimental section, additional characterization, theoretical calculation analysis (Figures S1−S17) (PDF)

■ AUTHOR INFORMATION

Corresponding Author

Kanta Ogawa − *Department of Materials, Imperial College London, London SW7 2AZ, U.K.;* orcid.org/0000-0002-6995-9848; Email: k.ogawa@imperial.ac.uk

Authors

Ryu Abe − *Department of Energy and Hydrocarbon Chemistry, Graduate School of Engineering, Kyoto University, Kyoto 615-8510, Japan;* orcid.org/0000-0001-8592-076X

Aron Walsh − *Department of Materials, Imperial College London, London SW7 2AZ, U.K.;* orcid.org/0000-0001-5460-7033

Complete contact information is available at: https://pubs.acs.org/10.1021/jacs.4c00150

Notes

The authors declare no competing financial interest.

■ ACKNOWLEDGMENTS

This work was financially supported by JSPS KAKENHI Grant-in-Aid for Scientific Research (A) (JP20H00398), JSPS Research Fellow (Grant Number 19J23357), and the JSPS overseas program. We are grateful to Dr. Takaaki Toriyama of Kyushu University for his helpful support in STEM analysis. Via our membership of the UK's HEC Materials Chemistry Consortium, which is funded by EPSRC (EP/X035859/1), this work used the ARCHER2 UK National Supercomputing Service (http://www.archer2.ac.uk).

■ REFERENCES

(1) Walsh, A.; Payne, D. J.; Egdell, R. G.; Watson, G. W. Stereochemistry of Post-Transition Metal Oxides: Revision of the Classical Lone Pair Model. *Chem. Soc. Rev.* **2011**, *40*, 4455.

(2) Kojima, A.; Teshima, K.; Shirai, Y.; Miyasaka, T. Organometal Halide Perovskites as Visible-Light Sensitizers for Photovoltaic Cells. *J. Am. Chem. Soc.* **2009**, *131*, 6050−6051.

(3) Diehl, L.; Bette, S.; Pielnhofer, F.; Betzler, S.; Moudrakovski, I.; Ozin, G. A.; Dinnebier, R.; Lotsch, B. V. Structure-Directing Lone Pairs: Synthesis and Structural Characterization of $SnTiO_3$. *Chem. Mater.* **2018**, *30*, 8932−8938.

(4) Ogawa, K.; Suzuki, H.; Zhong, C.; Sakamoto, R.; Tomita, O.; Saeki, A.; Kageyama, H.; Abe, R. Layered Perovskite Oxyiodide with Narrow Band Gap and Long Lifetime Carriers for Water Splitting Photocatalysis. *J. Am. Chem. Soc.* **2021**, *143*, 8446−8453.

(5) Brandt, R. E.; Stevanović, V.; Ginley, D. S.; Buonassisi, T. Identifying Defect-Tolerant Semiconductors with High Minority-Carrier Lifetimes: Beyond Hybrid Lead Halide Perovskites. *MRS Commun.* **2015**, *5*, 265−275.

(6) Kadowaki, H.; Saito, N.; Nishiyama, H.; Kobayashi, H.; Shimodaira, Y.; Inoue, Y. Overall Splitting of Water by RuO_2 -Loaded $PbWO_4$ Photocatalyst with $d^{10}s^2$-d^0 Configuration. *J. Phys. Chem. C* **2007**, *111*, 439−444.

(7) Minohara, M.; Dobashi, Y.; Kikuchi, N.; Samizo, A.; Honda, T.; He, X.; Katase, T.; Kamiya, T.; Nishio, K.; Aiura, Y. Tuning of Hole Carrier Density in P-Type α-$SnWO_4$ by Exploiting Oxygen Defects. *Mater. Adv.* **2022**, *3*, 9111−9116.

(8) Kudo, A.; Omori, K.; Kato, H. A Novel Aqueous Process for Preparation of Crystal Form-Controlled and Highly Crystalline $BiVO_4$ Powder from Layered Vanadates at Room Temperature and Its Photocatalytic and Photophysical Properties. *J. Am. Chem. Soc.* **1999**, *121*, 11459−11467.

(9) Walsh, A.; Yan, Y.; Huda, M. N.; Al-Jassim, M. M.; Wei, S.-H. Band Edge Electronic Structure of $BiVO_4$: Elucidating the Role of the Bi s and V d Orbitals. *Chem. Mater.* **2009**, *21*, 547−551.

(10) Fujito, H.; Kunioku, H.; Kato, D.; Suzuki, H.; Higashi, M.; Kageyama, H.; Abe, R. Layered Perovskite Oxychloride Bi_4NbO_8Cl: A Stable Visible Light Responsive Photocatalyst for Water Splitting. *J. Am. Chem. Soc.* **2016**, *138*, 2082−2085.

(11) Kunioku, H.; Higashi, M.; Tomita, O.; Yabuuchi, M.; Kato, D.; Fujito, H.; Kageyama, H.; Abe, R. Strong Hybridization between Bi-6s and O-2p Orbitals in Sillén−Aurivillius Perovskite Bi_4MO_8X (M = Nb, Ta; X = Cl, Br), Visible Light Photocatalysts Enabling Stable Water Oxidation. *J. Mater. Chem. A* **2018**, *6*, 3100−3107.

(12) Kuriki, R.; Ichibha, T.; Hongo, K.; Lu, D.; Maezono, R.; Kageyama, H.; Ishitani, O.; Oka, K.; Maeda, K. A Stable, Narrow-Gap Oxyfluoride Photocatalyst for Visible-Light Hydrogen Evolution and Carbon Dioxide Reduction. *J. Am. Chem. Soc.* **2018**, *140*, 6648−6655.

(13) Mohn, C. E.; Stølen, S. Influence of the Stereochemically Active Bismuth Lone Pair Structure on Ferroelectricity and Photocalytic Activity of Aurivillius Phase Bi_2WO_6. *Phys. Rev. B* **2011**, *83*, No. 014103.

(14) Abrahams, I.; Clark, S. J.; Donaldson, J. D.; Khan, Z. I.; Southern, J. T. Hydrolysis of Tin(II) Fluoride and Crystal Structure of Sn_4OF_6. *J. Chem. Soc., Dalton Trans.* **1994**, No. 17, 2581.

(15) Charkin, D. O.; Akinfiev, V. S.; Alekseeva, A. M.; Batuk, M.; Abakumov, A. M.; Kazakov, S. M. Synthesis and Cation Distribution in the New Bismuth Oxyhalides with the Sillén−Aurivillius Intergrowth Structures. *Dalton Trans.* **2015**, *44*, 20568−20576.

(16) Ok, K. M. Functional Layered Materials with Heavy Metal Lone Pair Cations, Pb^{2+}, Bi^{3+}, and Te^{4+}. *Chem. Commun.* **2019**, *55*, 12737−12748.

(17) Ogawa, K.; Tolborg, K.; Walsh, A. Models of Oxygen Occupancy in Lead Phosphate Apatite $Pb_{10}(PO_4)_6O$. *ACS Energy Lett.* **2023**, *8*, 3941−3944.
(18) Minohara, M.; Nemoto, Y.; Asanuma, S.; Hase, I.; Aiura, Y. Destabilization of $Sn^{2+}5s^2$ Lone-Pair States of SnO through Dimensional Crossover. *J. Phys. Chem. Lett.* **2023**, *14*, 5985−5992.
(19) Walsh, A.; Watson, G. W.; Payne, D. J.; Edgell, R. G.; Guo, J.; Glans, P.-A.; Learmonth, T.; Smith, K. E. Electronic Structure of the α and δ Phases of Bi_2O_3: A Combined *Ab Initio* and x-Ray Spectroscopy Study. *Phys. Rev. B* **2006**, *73*, 235104.
(20) Borowska-Centkowska, A.; Liu, X.; Krynski, M.; Leszczynska, M.; Wrobel, W.; Malys, M.; Hull, S.; Norberg, S. T.; Krok, F.; Abrahams, I. Defect Structure in δ-$Bi_5PbY_2O_{11.5}$. *RSC Adv.* **2019**, *9*, 9640−9653.
(21) Stoltzfus, M. W.; Woodward, P. M.; Seshadri, R.; Klepeis, J.-H.; Bursten, B. Structure and Bonding in $SnWO_4$, $PbWO_4$, and $BiVO_4$: Lone Pairs vs Inert Pairs. *Inorg. Chem.* **2007**, *46*, 3839−3850.
(22) Lundegaard, L. F.; Makovicky, E.; Boffa-Ballaran, T.; Balic-Zunic, T. Crystal Structure and Cation Lone Electron Pair Activity of Bi_2S_3 between 0 and 10 GPa. *Phys. Chem. Minerals* **2005**, *32*, 578−584.
(23) Olsen, L. A.; López-Solano, J.; García, A.; Balić-Žunić, T.; Makovicky, E. Dependence of the Lone Pair of Bismuth on Coordination Environment and Pressure: An Ab Initio Study on $Cu_4Bi_5S_{10}$ and Bi_2S_3. *J. Solid State Chem.* **2010**, *183*, 2133−2143.
(24) Shannon, R. D. Revised Effective Ionic Radii and Systematic Studies of Interatomie Distances in Halides and Chaleogenides. *Acta Crystallogr.* **1976**, *32*, 751−767.
(25) Jain, A.; Ong, S. P.; Hautier, G.; Chen, W.; Richards, W. D.; Dacek, S.; Cholia, S.; Gunter, D.; Skinner, D.; Ceder, G.; Persson, K. A. Commentary: The Materials Project: A Materials Genome Approach to Accelerating Materials Innovation. *APL Materials* **2013**, *1*, No. 011002.
(26) Waroquiers, D.; Gonze, X.; Rignanese, G.-M.; Welker-Nieuwoudt, C.; Rosowski, F.; Göbel, M.; Schenk, S.; Degelmann, P.; André, R.; Glaum, R.; Hautier, G. Statistical Analysis of Coordination Environments in Oxides. *Chem. Mater.* **2017**, *29*, 8346−8360.
(27) Schmidt, M.; Oppermann, H.; Hennig, C. Untersuchungen zu Bismutseltenerdoxidhalogeniden der Zusammensetzung Bi_2SEO_4X (X = Cl, Br, I). *Z. Anorg. Allg. Chem.* **2000**, *626*, 125−135.
(28) Nakada, A.; Kato, D.; Nelson, R.; Takahira, H.; Yabuuchi, M.; Higashi, M.; Suzuki, H.; Kirsanova, M.; Kakudou, N.; Tassel, C.; Yamamoto, T.; Brown, C. M.; Dronskowski, R.; Saeki, A.; Abakumov, A.; Kageyama, H.; Abe, R. Conduction Band Control of Oxyhalides with a Triple-Fluorite Layer for Visible Light Photocatalysis. *J. Am. Chem. Soc.* **2021**, *143*, 2491−2499.
(29) Dronskowski, R.; Bloechl, P. E. Crystal Orbital Hamilton Populations (COHP): Energy-Resolved Visualization of Chemical Bonding in Solids Based on Density-Functional Calculations. *J. Phys. Chem.* **1993**, *97*, 8617−8624.
(30) Ogawa, K.; Suzuki, H.; Walsh, A.; Abe, R. Orbital Engineering in Sillén−Aurivillius Phase Bismuth Oxyiodide Photocatalysts through Interlayer Interactions. *Chem. Mater.* **2023**, *35*, 5532−5540.
(31) Huang, Y.-T.; Kavanagh, S. R.; Scanlon, D. O.; Walsh, A.; Hoye, R. L. Z. Perovskite-Inspired Materials for Photovoltaics and beyond—from Design to Devices. *Nanotechnology* **2021**, *32*, 132004.
(32) Jiang, Y.; Mi, Y.; Li, C.; Fang, W.; Li, X.; Zeng, X.; Liu, Y.; Shangguan, W. Solid-Phase Synthesis of $Bi_{3-x}Y_xO_4Cl$ Solid Solution for Visible-Light Photocatalytic Hydrogen Generation. *J. Alloys Compd.* **2021**, *884*, 161036.
(33) Zhou, W.; Umezawa, N. Band Gap Engineering of Bulk and Nanosheet SnO: Insight into the Interlayer Sn-Sn Lone Pair Interactions. *Phys. Chem. Chem. Phys.* **2015**, *17*, 17816−17820.

https://doi.org/10.1021/jacs.4c00150
J. Am. Chem. Soc. 2024, 146, 5806−5810